


Incommensurate Spin Density Wave in Antiferromagnetic RuO₂ Evinced by Abnormal Spin Splitting Torque

Xiaoyu Feng,¹ Hua Bai²,^{*} Xinxin Fan,¹ Muhan Guo,¹ Zhiqiang Zhang,¹ Guozhi Chai²,
Tao Wang,¹ Desheng Xue,¹ Cheng Song,² and Xiaolong Fan^{1,*}

¹Key Laboratory of Magnetism and Magnetic Materials (MOE), School of Physics Science and Technology, Lanzhou University, Lanzhou 730000, China

²Key Laboratory of Advanced Materials (MOE), School of Materials Science and Engineering, Tsinghua University, Beijing 100084, China

 (Received 13 August 2023; revised 17 December 2023; accepted 23 January 2024; published 21 February 2024)

Since the discovery of antiferromagnetism, metallic oxide RuO₂ has exhibited numerous intriguing spintronics properties such as the anomalous Hall effect and anisotropic spin splitting effect. However, the microscopic origin of its antiferromagnetism remains unclear. By investigating the spin splitting torque in RuO₂/Py, we found that metallic RuO₂ exhibits a spatially periodic spin structure which interacts with the spin waves in Py through interfacial exchange coupling. The wavelength of such structure is evaluated within 14–20 nm depending on the temperature, which is evidence of an incommensurate spin density wave state in RuO₂. Our work not only provides a dynamics approach to characterize the antiferromagnetic ordering in RuO₂, but also offers fundamental insights into the spin current generation due to anisotropic spin splitting effect associated with spin density wave.

DOI: [10.1103/PhysRevLett.132.086701](https://doi.org/10.1103/PhysRevLett.132.086701)

The 4*d* transition metal oxide RuO₂ has long been considered a Pauli paramagnet, and because of its relatively high electrical conductivity and thermal stability, it plays an important role in the field of technical applications [1]. Recently, some experimental results have confirmed that RuO₂ has antiferromagnetic (AFM) order at least 300 K, which lays the foundation for its potential application in antiferromagnetic spintronics [2–6]. For instance, the combination of its unique electron structure and antiferromagnetism enables the efficient spin current generation [7–9]. As shown in Figs. 1(a) and 1(b), with the rutile crystal structure, RuO₂ exhibits two magnetic sublattices being rotated with respect to each other by 90° [7]. The momentum-dependent anisotropic spin-splitting energy band in RuO₂ can directly interact with the external electric field to generate spin current, known as the anisotropic spin splitting effect (ASSE) [4]. The ASSE provides a fundamental spin current generation approach that is independent of relativistic spin-orbit coupling and the spin polarization is parallel to the Néel vector rather than perpendicular to the trajectory of electrons, which has been verified by plenty of works [10–13]. This exotic physical phenomenon provides the feasibility for tunable spin splitting torque (SST) through control of the Néel vector in RuO₂.

However, the microscopic origin of antiferromagnetism in metallic RuO₂ remains inconclusive [2,3]. Theoretical studies suggest that itinerant antiferromagnetism in RuO₂ may arise from the instability due to Fermi surface nesting [2,14], where a spin density wave (SDW) state manifests itself as a real-space spin modulation [15–17].

The spatial period of the SDW can be either commensurate (C) or incommensurate (IC) with the lattice constant [17,18], as shown in Figs. 1(c) and 1(d). So far, the AFM order in bulk RuO₂ has been observed with a commensurate magnetic propagation vector $Q_{\text{AFM}} = (1, 0, 0)$ using neutron and x-ray resonant magnetic diffraction [2,3]. However, the C-SDW [Fig. 1(c)] can also be described within a local moment picture with antiferromagnet exchange coupling, making it difficult to confirm whether the itinerant AFM state in RuO₂ originates from SDW or not. Therefore, finding evidence of IC-SDW [Fig. 1(d)] is crucial in confirming the source of antiferromagnetism in RuO₂.

In this Letter, we present evidence of the IC-SDW in RuO₂/Py heterostructures by investigating the temperature and frequency-dependent spin dynamics in Py. The key factor in our study is the interfacial exchange coupling (IEC) between RuO₂ and Py: (1) the IEC results in the presence of IC-SDW in RuO₂, similar to the transformation of the SDW from C to IC in Cr/FM bilayers [19,20]; (2) together with IEC, the spatial modulation of the Néel vector in RuO₂ leads to a periodic pinning on Py, which can interact with the spin waves in Py through Bragg scattering and has been detected as the anomaly in the spin dynamics of Py. Our experimental results show the temperature dependence of the SDW wave vector in RuO₂/Py, and we estimate the corresponding λ_{SDW} in the range of 14–20 nm, providing experimental evidence supporting the theoretical prediction that the AFM order in RuO₂ originate from an itinerant SDW state [2].

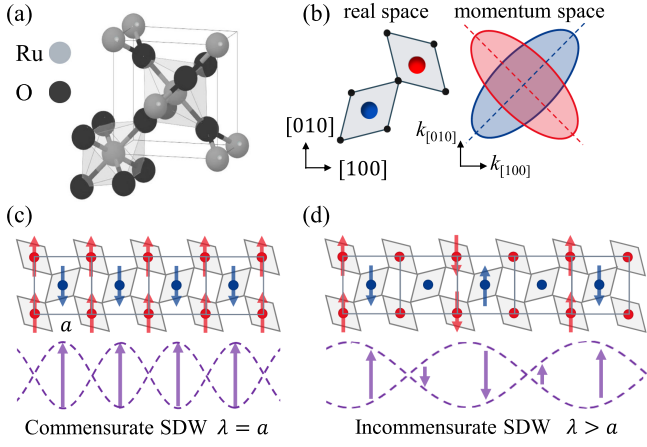


FIG. 1. (a) Crystal structure of RuO_2 . (b) Top view of the RuO_2 with opposite spin directions on two magnetic sublattices in real space (left) and momentum space (right). (c) C-SDW and (d) IC-SDW in RuO_2 . The red and blue spheres (arrows) represent Ru atoms (spin orientations) in alternative magnetic sublattices. Purple arrows represent the Néel vector in a unit cell and dash lines characterize spin amplitude of SDW in real space.

We begin our experiments by investigating the IEC in $\text{RuO}_2(12 \text{ nm})/\text{Py}(8 \text{ nm})$. We deposited (100)- and (110)-oriented RuO_2 films onto SrTiO_3 (STO) (100) and MgO (100) substrates using magnetron sputtering. The results of x-ray diffraction indicated that the RuO_2 films exhibited strong (100) and (110) texture with a multidomain distribution within the plane. The detailed analysis of the crystal structure is depicted in Sec. S1 of Supplemental Material [21]. After magnetic field annealing, both samples show exchange bias, as is evident from the hysteresis loops shown in Fig. 2(a) (see Supplemental Material, Sec. S2 [21]). Interestingly, the exchange bias field H_{EB} in $\text{RuO}_2(100)/\text{Py}$ changes sign around 70 K, while the amplitude of H_{EB} in $\text{RuO}_2(110)/\text{Py}$ increases monotonously with decreasing temperature. The behavior of H_{EB} in RuO_2/Py , with the sign reversal and dependence on certain crystal orientation, is difficult to understand based on AFM materials with localized moments (e.g., CoO , IrMn , etc.) [31,32]. However, such characteristics are common in IC-SDW AFM systems [e.g., $\text{Cr}(100)/\text{Py}$] [33,34]. Considering the results of Berlijn *et al.* that itinerant antiferromagnetism in RuO_2 is attributed to SDW arising from Fermi surface instability [2], the data shown in Fig. 2(b) could indicate the presence of IC-SDW in RuO_2/Py .

In the following, we try to double-check the evidence of the IC-SDW and estimate the SDW wavelength λ_{SDW} through investigating the details of spin dynamics in RuO_2/Py by using spin-torque ferromagnetic resonance (ST FMR). Unlike spin Hall effect (SHE) or noncollinear magnetic order induced spin currents, the flowing direction of the spin current generated by the ASSE is determined by the angle between the electric field and the anisotropic axes of the energy bands, with the spin polarization direction

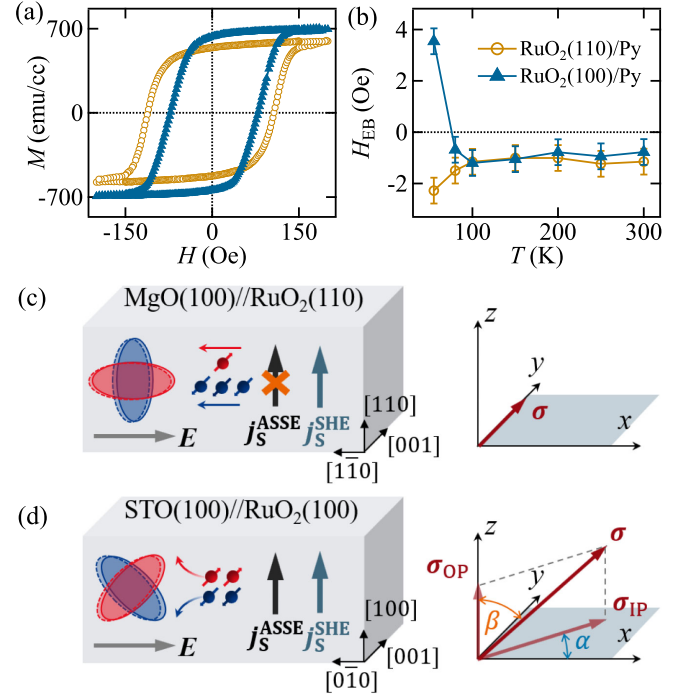


FIG. 2. (a) Hysteresis loops and (b) temperature dependent H_{EB} for $\text{RuO}_2(110)/\text{Py}$ (yellow) and $\text{RuO}_2(100)/\text{Py}$ (blue) at $T = 55 \text{ K}$. (c) The transversal spin current comes only from the SHE of $\text{RuO}_2(110)$ with $E \parallel [\bar{1}10]$ and the $\sigma \parallel \hat{y}$. (d) For $\text{RuO}_2(100)$ with $E \parallel [010]$, both ASSE and SHE can generate transversal spin current with arbitrary σ which was decomposed into σ_{IP} (α with respect to \hat{x}) and σ_{OP} (β to \hat{z}).

parallel to the Néel vector [4,35]. When an electric field $E \parallel [\bar{1}10]$ within the (110)-oriented film, only longitudinal spin-polarized current parallel to the E is generated, as shown in Fig. 2(c). Therefore, in $\text{RuO}_2(110)/\text{Py}$, the magnetization of Py is only excited by the spin current of SHE with the spin polarization $\sigma \parallel \hat{y}$. In contrast, in $\text{RuO}_2(100)/\text{Py}$, a transverse spin current j_S perpendicular to the E can be generated when the $E \parallel [010]$, as shown in Fig. 2(d) [10,12]. Therefore, both ASSE and SHE would excite the magnetization of Py through SST and spin orbit torque (SOT).

Considering that the spin polarization σ of the spin current from ASSE is parallel to the Néel vector, and the Néel vector of the $\text{STO} \parallel \text{RuO}_2(100)$ thin film does not strictly align with the easy axis ([001] or the \hat{y} axis) [3,6], we decomposed the σ into in-plane σ_{IP} (α with respect to \hat{x}) and out-of-plane components σ_{OP} (β to \hat{z}), as shown in Fig. 2(d).

Next, we employed the variable-temperature ST FMR for determining the direction of σ , as an indirect approach for probing the Néel order in RuO_2 , the details of the device fabrication and measurement setup are introduced in Supplemental Material, Sec. S3 [21]. Figures 3 show the frequency-dependent ST FMR spectra of $\text{RuO}_2(110)/\text{Py}$, $\text{RuO}_2(100)/\text{Cu}/\text{Py}$, and $\text{RuO}_2(100)/\text{Py}$ at 100 K. For the

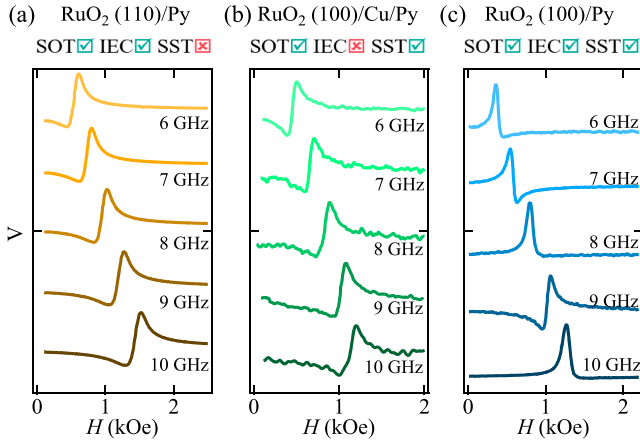


FIG. 3. ST FMR spectra of RuO₂(110)/Py, RuO₂(100)/Cu/Py and RuO₂(100)/Py at $T = 100$ K, 20 dBm, magnetic field is applied in device plane with 45° respect to dynamics current.

last sample where both SST and IEC presents, the resonant line shape exhibits distinct frequency-dependent behavior which is unusual in ST FMR experiments [22,23]. The frequency-dependent line shape measured at different temperatures is summarized in Sec. S4 [21]. However, for RuO₂(110)/Py (without SST) and RuO₂(100)/Cu/Py (without IEC), the line shape remains unchanged. Phenomenologically, the abnormal frequency-dependent line shape is a consequence of the simultaneous presence of SST and IEC.

Based on the theory of ST FMR, the line shape is almost frequency independent [22]. Considering the complicity of the multiple physical effects and microwave transmission in coplanar waveguide (CPW) device, the frequency-dependent line shape could result from the following factors: (1) multiple signal sources related to FMR, such as inverse SHE caused by spin pumping or resonance thermal effects [36,37]; (2) impedance mismatch of CPW device, which would result in frequency-dependent distribution of the microwave magnetic field \mathbf{h} and the phase between the dynamic current \mathbf{j}_C and \mathbf{h} [24,38]. However, those factors can be excluded by comparing the experimental results of RuO₂(110)/Py, RuO₂(100)/Cu/Py, and controlled sample Pt/Py with the same device structure and fabrication process (Sec. S3 [21]). On the other hand, if the Py magnetization is only excited by \mathbf{j}_C through SOT and SST, the line shape depends on the $\sigma(\alpha, \beta)$ of spin current and the ratio of real $\text{Re}[G_{\uparrow\downarrow}]$ and imaginary $\text{Im}[G_{\uparrow\downarrow}]$ part of the spin mixing conductance [39]. Therefore, considering the $\text{Re}[G_{\uparrow\downarrow}]$, $\text{Im}[G_{\uparrow\downarrow}]$ and the spin Hall angle in RuO₂ are independent of the microwave frequency f_{FMR} , the abnormal frequency-dependent line shape in RuO₂(100)/Py should be attributed to the fact that the spin polarization σ as well as the Néel order in RuO₂ undergo significant impact with frequency.

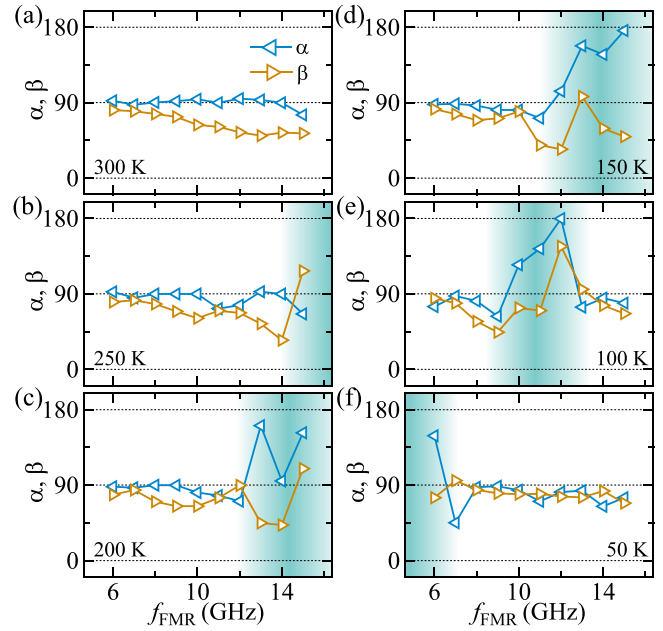


FIG. 4. (a)–(f) The angle α (blue) and β (yellow) of $\sigma(\alpha, \beta)$, plotted as a function of f_{FMR} for RuO₂(100)/Py with temperature $T = 300, 250, 200, 150, 100, 50$ K. The green shadow represents the frequency band where ST FMR line shape as well as $\sigma(\alpha, \beta)$ show dramatically change.

To quantify the frequency-dependent $\sigma(\alpha, \beta)$ in RuO₂(100)/Py, the ST FMR spectra are measured as a function of the angle θ between the \mathbf{H} and \mathbf{j}_C in the device plane. By identifying spatial symmetry of spin torques in Py, the α and β can be evaluated as a function of frequency at different temperature (Sec. S5 [21]). As shown in Fig. 4(a), α and β remain almost constant at 300 K. However, when $T \leq 250$ K, α and β dramatically change in a certain frequency band, and the central frequency of the band decreases with decreasing temperature. At 100 K, a whole band can be observed within our tested frequency range of 6–15 GHz. At 50 K, the band center is below 6 GHz, and we can observe a recovery of α and β to the initial state when $f_{\text{FMR}} > 8$ GHz. On the other hand, $\sigma(\alpha, \beta)$ of RuO₂(110)/Py and RuO₂(100)/Cu/Py is independent on frequency and temperature (Figs. S6 and S8 [21]). Therefore, from the data shown in Figs. 3 and 4 it is evident that the σ (or the Néel vector) in RuO₂/Py undergoes a dramatic change within a frequency band once both SST and IEC are present.

Typically, in the presence of gigahertz microwave excitation, the Néel vector does not respond significantly. We attribute the abnormal frequency-dependent behavior of $\sigma(\alpha, \beta)$ to the interaction between the spin waves in Py and the SDW at the RuO₂ surface through IEC, as illustrated in Fig. 5(a). The dispersion relation of the spin waves in Py is given by [40]

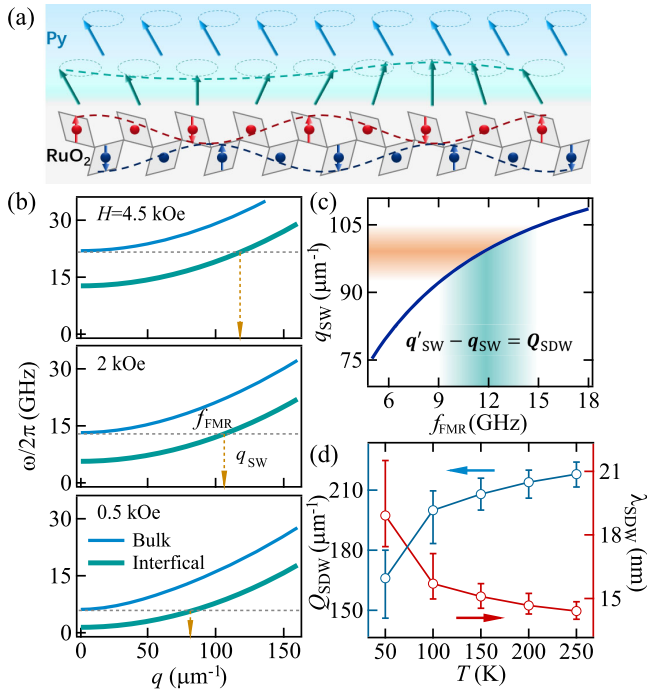


FIG. 5. (a) The blue arrows in Py indicates the FMR mode (f_{FMR} , $q = 0$), the green arrows represent the interfacial SW mode at the interface (f_{FMR} , q_{SW}). The blue and red dash lines in RuO₂ represent the IC-SDW for each sublattice. For clear illustration, the magnetic moment in Py and RuO₂ are set perpendicular to the interface. (b) The spin wave dispersion of bulk Py (blue) and interfacial Py (green). The gray dashed lines define f_{FMR} at different magnetic field. (c) Calculated relation between q_{SW} and f_{FMR} . (d) Q_{SDW} (left) and λ_{SDW} (right) for different temperature.

$$\omega(q) = \gamma \sqrt{\left(H + \frac{Dq^2}{\gamma\hbar}\right) \left(H + 4\pi M_{\text{eff}} + \frac{Dq^2}{\gamma\hbar}\right)},$$

where $\gamma/2\pi = 2.8$ GHz/kOe is the gyromagnetic ratio, D is the exchange stiffness constant (4.29×10^{-40} Jm² for Py), \hbar is the reduced Planck constant, H is the applied magnetic field. Considering the presence of interfacial defects or exchange coupling that pin the magnetic moments of Py at the RuO₂/Py interface [25,26,41], there is a distribution of the effective demagnetization field $4\pi M_{\text{eff}}$ of each Py moment along the thickness direction, so that the spin wave dispersion is also distributed. Because only the moments near the interface are crucial for dealing with the coupling between Py and RuO₂, we consider two extreme spin wave modes, namely bulk mode (away from interface with maximum $4\pi M_{\text{eff}} \approx 4\pi M_s$) and interfacial mode (with minimum $4\pi M_{\text{eff}} \approx 0$) to simplify the distribution of the SW dispersion relation as illustrated in Fig. 5(b). More detail can be found in Sec. S6 [21]. Since only the FMR mode ($q = 0$) can be detected by the mixing voltage in ST FMR experiments, every time when a resonance peak of bulk

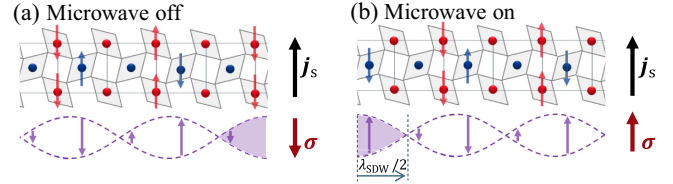


FIG. 6. One possible consequence of the interaction between spin waves and SDW. The purple shadow indicates the uncanceled Néel vector.

FMR is detected, there is an interfacial spin wave mode ($q_{\text{SW}} \neq 0$) that is excited simultaneously at the same frequency f_{FMR} . Here, q_{SW} is defined as the wave vector of a specific interfacial spin wave with the same frequency as f_{FMR} as indicated by the yellow arrows in Fig. 5(b). q_{SW} increase with the f_{FMR} (or H), and their relationship is summarized in Fig. 5(c).

Therefore, when the SDW wave vector Q_{SDW} and the q_{SW} of the interfacial spin waves satisfy the Bragg reflection condition $q'_{\text{SW}} - q_{\text{SW}} = Q_{\text{SDW}}$ [42], interference occurs. The momentum of the spin waves in Py can effectively transfer to the SDW in RuO₂, thereby altering the state of the SDW, which is similar to the periodic magnetic domain structure controlled by spin waves through momentum transfer torque [43,44]. To visualize this interaction, we consider a RuO₂ grain with the length of $2.5\lambda_{\text{SDW}}$ as shown in Fig. 6 [27,28]. If the spin waves make the SDW move forward for half wavelength, the effective Néel vector (purple shadow) would be reversed. Considering that the spin polarization of ASSE generated spin current is only determined by the direction of Néel vector, such a movement of SDW would result in a reversal of σ as well as the resonant line shape of ST FMR spectra. More discussion can be found in Sec. S7 [21].

In general, for a given value of Q_{SDW} , there exists a distribution of q_{SW} that satisfies the Bragg condition (Sec. S8 [21]). Because of the relationship shown in Fig. 5(c), the distribution of q_{SW} leads to a specific frequency band of f_{FMR} [29,30]. Within the band, interference between the spin waves and the SDW occurs, which explains the observed abnormality of the line shape [or $\sigma(\alpha, \beta)$] shown before. As indicated by the shaded region in Fig. 5(c), the band center corresponds to q_{SW} at $100 \mu\text{m}^{-1}$ at 100 K. Therefore, the Q_{SDW} is in the same order of q_{SW} with a wavelength in the tens of nanometers range, which is significantly larger than the lattice constant of RuO₂, indicating the presence of IC-SDW at the RuO₂ interface.

Note that in previous experiments using neutron diffraction and resonant x-ray scattering, no significant IC-SDW wave vector Q_{SDW} was observed in RuO₂ [2,3]. Therefore, even if SDW exists in RuO₂, the previous experimental results could not provide definitive evidence. Unlike the bulk RuO₂, what we observed is the behavior of IC-SDW at the interface, where the IEC at the RuO₂/Py interface plays a

crucial role. First, under the action of the IEC, the neighboring magnetic layer Py enables the C-SDW transition to the IC-SDW near the RuO₂ interface [19,20,45,46]. Second, in combination with the IC-SDW, the IEC periodically pins the interfacial magnetic moments of Py, allowing for interference between the spin waves and the SDW, thereby result in the observed transition in $\sigma(\alpha, \beta)$ at specific band. Consequently, the detection of those band makes it possible to estimate the evaluate of Q_{SDW} and λ_{SDW} . Based on the central frequency of the band in Fig. 4, we use one-dimensional lattice mode for estimating the temperature dependent Q_{SDW} and λ_{SDW} , namely $2|q_{\text{SW}}| = |Q_{\text{SDW}}| = \pi/\lambda_{\text{SDW}}$ [47], as shown in Fig. 5(d). According to $\lambda_{\text{SDW}} = a/\delta$, where δ is the incommensurability parameter of SDW [46,48], a is the lattice constant ($a = b = 4.5 \text{ \AA}$, $c = 3.1 \text{ \AA}$ for tetragonal RuO₂), we found δ to be around 0.02–0.03, which agrees with values of SDW materials [18,48,49].

Additionally, it can be observed that λ_{SDW} increases as the temperature decreases, which is consistent with other experimental results [50,51]. However, since the temperature dependent magnetic and structural parameters of RuO₂ are missing, theoretical estimation of $\lambda_{\text{SDW}}(T)$ is still open. Nevertheless, the polarity reversal of H_{EB} shown in Fig. 2(b) could be linked to the reversal of the effective Néel vectors at RuO₂/Py interface due to the temperature dependent λ_{SDW} [33,34]. Consequently, the reversal of SST triggered only by the temperature is realized, see Sec. S9 for more details.

To conclude, based on the Bragg reflection condition, we propose a model for the interaction between spin waves and SDW through IEC, and estimate the wavelength of the periodic structure to be 14–20 nm, providing evidence of the existence of IC-SDW in RuO₂. Our work not only deepen the understanding of the source of antiferromagnetism in RuO₂, but also provide a dynamic approach to characterize the SDW properties in RuO₂ thin films. Meanwhile, the interaction between spin waves and SDW could be utilized for manipulate the effective Néel vector as well as the SST in RuO₂/FM heterostructures, which is useful for exploring more flexible spintronics device based on spin torque.

The authors thank Peng Yan, Chenglong Jia, and Qingfang Liu for their helpful discussions. This work is supported by the National Natural Science Foundation of China (Grants No. 52171231 and No. 12174165) and the 111 Project under Grant No. B20063.

*fanxiaolong@lzu.edu.cn

- [1] S. Trasatti, *Electrodes and Conductive Metallic Oxides* (Elsevier, New York, 1980).
 [2] T. Berlijn, P. C. Snijders, O. Delaire, H. D. Zhou, T. A. Maier, H. B. Cao, S. X. Chi, M. Matsuda, Y. Wang,

- M. R. Koehler, P. R. C. Kent, and H. H. Weitering, Itinerant antiferromagnetism in RuO₂, *Phys. Rev. Lett.* **118**, 077201 (2017).
 [3] Z. H. Zhu, J. Stremper, R. R. Rao, C. A. Occhialini, J. Pellicciari, Y. Choi, T. Kawaguchi, H. You, J. F. Mitchell, Y. Shao-Horn, and R. Comin, Anomalous antiferromagnetism in metallic RuO₂ determined by resonant x-ray scattering, *Phys. Rev. Lett.* **122**, 017202 (2019).
 [4] R. Gonzalez-Hernandez, L. Smejkal, K. Vyborny, Y. Yahagi, J. Sinova, T. Jungwirth, and J. Zelezny, Efficient electrical spin splitter based on nonrelativistic collinear antiferromagnetism, *Phys. Rev. Lett.* **126**, 127701 (2021).
 [5] Z. Feng, X. Zhou, L. Šmejkal, L. Wu, Z. Zhu, H. Guo, R. González-Hernández, X. Wang, H. Yan, P. Qin, X. Zhang, H. Wu, H. Chen, Z. Meng, L. Liu, Z. Xia, J. Sinova, T. Jungwirth, and Z. Liu, An anomalous Hall effect in altermagnetic ruthenium dioxide. *National electronics review* **5**, 735 (2022).
 [6] X. Zhou, W. Feng, R. Zhang, L. Šmejkal, J. Sinova, Yuriy Mokrousov, and Y. Yao, Crystal thermal transport in altermagnetic RuO₂, *Phys. Rev. Lett.* **132**, 056701 (2024).
 [7] L. Šmejkal, J. Sinova, and T. Jungwirth, Emerging research landscape of altermagnetism, *Phys. Rev. X* **12**, 040501 (2022).
 [8] D. F. Shao, S. H. Zhang, M. Li, C. B. Eom, and E. Y. Tsymlal, Spin-neutral currents for spintronics, *Nat. Commun.* **12**, 7061 (2021).
 [9] D. F. Shao, Y. Y. Jiang, J. Ding, S. H. Zhang, Z. A. Wang, R. C. Xiao, G. Gurung, W. J. Lu, Y. P. Sun, and E. Y. Tsymlal, Néel spin currents in antiferromagnets, *Phys. Rev. Lett.* **130**, 216702 (2023).
 [10] H. Bai, L. Han, X. Y. Feng, Y. J. Zhou, R. X. Su, Q. Wang, L. Y. Liao, W. X. Zhu, X. Z. Chen, F. Pan, X. L. Fan, and C. Song, Observation of spin splitting torque in a collinear antiferromagnet RuO₂, *Phys. Rev. Lett.* **128**, 197202 (2022).
 [11] H. Bai, Y. C. Zhang, Y. J. Zhou, P. Chen, C. H. Wan, L. Han, W. X. Zhu, S. X. Liang, Y. C. Su, X. F. Han, F. Pan, and C. Song, Efficient spin-to-charge conversion via altermagnetic spin splitting effect in antiferromagnet RuO₂, *Phys. Rev. Lett.* **130**, 216701 (2023).
 [12] S. Karube, T. Tanaka, D. Sugawara, N. Kadoguchi, M. Kohda, and J. Nitta, Observation of spin-splitter torque in collinear antiferromagnetic RuO₂, *Phys. Rev. Lett.* **129**, 137201 (2022).
 [13] A. Bose, N. J. Schreiber, R. Jain, D. F. Shao, H. P. Nair, J. X. Sun, X. S. Zhang, D. A. Muller, E. Y. Tsymlal, D. G. Schlom, and D. C. Ralph, Tilted spin current generated by the collinear antiferromagnet ruthenium dioxide, *National Electron. Rev.* **5**, 267 (2022).
 [14] K.-H. Ahn, A. Hariki, K.-W. Lee, and J. Kuneš, Antiferromagnetism in RuO₂ as d -wave Pomeranchuk instability, *Phys. Rev. B* **99**, 184432 (2019).
 [15] E. Fawcett, Spin-density-wave antiferromagnetism in chromium, *Rev. Mod. Phys.* **60**, 209 (1988).
 [16] D. Qian, X. F. Jin, J. Barthel, M. Klaua, and J. Kirschner, Spin-density wave in ultrathin Fe films on Cu (100), *Phys. Rev. Lett.* **87**, 227204 (2001).
 [17] Y. Hu, T. Zhang, D. Zhao, C. Chen, S. Ding, W. Yang, X. Wang, C. Li, H. Wang, D. Feng, and T. Zhang, Real-space observation of incommensurate spin density wave and

- coexisting charge density wave on Cr (001) surface, *Nat. Commun.* **13**, 445 (2022).
- [18] D. K. Pratt, M. G. Kim, A. Kreyssig, Y. B. Lee, G. S. Tucker, A. Thaler, W. Tian, J. L. Zarestky, S. L. Bud'ko, P. C. Canfield, B. N. Harmon, A. I. Goldman, and R. J. McQueeney, Incommensurate spin-density wave order in electron-doped BaFe_2As_2 superconductors, *Phys. Rev. Lett.* **106**, 257001 (2011).
- [19] Z. P. Shi and R. S. Fishman, Interplay between spin-density wave and proximity magnetic layers, *Phys. Rev. Lett.* **78**, 1351 (1997).
- [20] A. Schreyer, C. F. Majkrzak, Th. Zeidler, T. Schmitte, P. Bödeker, K. Theis-Bröhl, A. Abromeit, J. A. Dura, and T. Watanabe, Magnetic structure of Cr in exchange coupled Fe/Cr (001) superlattices, *Phys. Rev. Lett.* **79**, 4914 (1997).
- [21] See Supplemental Material at <http://link.aps.org/supplemental/10.1103/PhysRevLett.132.086701> for the sample preparation and characterizations; interface exchange coupling characterization for RuO_2/Py ; ST FMR devices and spectrum fitting; seeing the abnormal frequency band through V_S/V_A ; angle-dependent ST FMR measurement; estimation of the interface anisotropy field at $\text{RuO}_2(100)/\text{Py}$ interface; collective excitation of SDW; distribution of q_{sw} ; reversal of STT triggered by temperature, which includes Refs. [3,6,10,22–30].
- [22] The statement is rigorous only if the influence of the applied magnetic field H to the orbital shape of magnetization precession was ignored, see L. Liu, T. Moriyama, D. C. Ralph, and R. A. Buhrman, Spin-torque ferromagnetic resonance induced by the spin Hall effect, *Phys. Rev. Lett.* **106**, 036601 (2011).
- [23] T. Nan, C. X. Quintela, J. Irwin, G. Gurung, D. F. Shao, J. Gibbons, N. Campbell, K. Song, S. Choi, L. Guo, R. D. Johnson, P. Manuel, R. V. Chopdekar, I. Hallsteinsen, T. Tybell, P. J. Ryan, J. Kim, Y. Choi, P. G. Radaelli, D. C. Ralph, E. Y. Tsybal, M. S. Rzchowski, and C. B. Eom, Controlling spin current polarization through non-collinear antiferromagnetism, *Nat. Commun.* **11**, 4671 (2020).
- [24] M. Harder, Y. Gui, and C.-M. Hu, Electrical detection of magnetization dynamics via spin rectification effects, *Phys. Rep.* **661**, 1 (2016).
- [25] R. Morales, Ali C. Basaran, J. E. Villegas, D. Navas, N. Soriano, B. Mora, C. Redondo, X. Battle, and Ivan K. Schuller, Exchange-bias phenomenon: The role of the ferromagnetic spin structure, *Phys. Rev. Lett.* **114**, 097202 (2015).
- [26] T. C. Schulthess and W. H. Butler, Coupling mechanisms in exchange biased films (invited), *J. Appl. Phys.* **85**, 5510 (1999).
- [27] G. Grüner, The dynamics of spin-density waves, *Rev. Mod. Phys.* **66**, 1 (1994).
- [28] P. C. Liao, Y. S. Huang, and K. K. Tiong, Characterization of RuO_2 and IrO_2 films deposited on Si substrate, *J. Alloys Compd.* **317**, 98 (2001).
- [29] H. Wang, R. Yuan, Y. Zhou, Y. Zhang, J. Chen, S. Liu, H. Jia, D. Yu, J. P. Ansermet, C. Song, and H. Yu, Long-distance coherent propagation of high-velocity antiferromagnetic spin waves, *Phys. Rev. Lett.* **130**, 096701 (2023).
- [30] U. K. Bhaskar, G. Talmelli, F. Ciubotaru, C. Adelman, and T. Devolder, Backward volume vs Damon–Eshbach: A traveling spin wave spectroscopy comparison, *J. Appl. Phys.* **127**, 033902 (2020).
- [31] N. J. Gökemeijer, R. L. Penn, D. R. Veblen, and C. L. Chien, Exchange coupling in epitaxial CoO/NiFe bilayers with compensated and uncompensated interfacial spin structures, *Phys. Rev. B* **63**, 174422 (2001).
- [32] G. Malinowski, M. Hehn, S. Robert, O. Lenoble, A. Schuhl, and P. Panissod, Magnetic origin of enhanced top exchange biasing in $\text{Py}/\text{IrMn}/\text{Py}$ multilayers, *Phys. Rev. B* **68**, 184404 (2003).
- [33] J. S. Parker, L. Wang, K. A. Steiner, P. A. Crowell, and C. Leighton, Exchange bias as a probe of the incommensurate spin-density wave in epitaxial Fe/Cr (001), *Phys. Rev. Lett.* **97**, 227206 (2006).
- [34] F. Y. Yang and C. L. Chien, Oscillatory exchange bias due to an antiferromagnet with incommensurate spin-density waves, *Phys. Rev. Lett.* **90**, 147201 (2003).
- [35] H. Y. Ma, M. Hu, N. Li, J. Liu, W. Yao, J. F. Jia, and J. Liu, Multifunctional antiferromagnetic materials with giant piezomagnetism and noncollinear spin current, *Nat. Commun.* **12**, 2846 (2021).
- [36] K. He, J. Cheng, M. Yang, Y. Zhang, L. Yu, Q. Liu, L. Sun, B. Miao, C. Hu, and H. Ding, Spin rectification effect induced by planar Hall effect and its strong impact on spin-pumping measurements, *Phys. Rev. B* **105**, 104406 (2022).
- [37] K. He, J. Cheng, M. Yang, L. Sun, W. Sun, S. Bedanta, A. Azevedo, B. Miao, and H. Ding, Spin rectification effects in ferromagnetic metal microstrips induced by anisotropic magnetoresistance, planar Hall effect, and anomalous Hall effect, *Phys. Rev. B* **106**, 104407 (2022).
- [38] A. Wirthmann, X. Fan, Y. S. Gui, K. Martens, G. Williams, J. Dietrich, G. E. Bridges, and C. M. Hu, Direct phase probing and mapping via spintronic Michelson interferometry, *Phys. Rev. Lett.* **105**, 017202 (2010).
- [39] A. Manchon, J. Železný, I. M. Miron, T. Jungwirth, J. Sinova, A. Thiaville, K. Garello, and P. Gambardella, Current-induced spin-orbit torques in ferromagnetic and antiferromagnetic systems, *Rev. Mod. Phys.* **91**, 035004 (2019).
- [40] T. G. Phillips and H. M. Rosenberg, Spin waves in ferromagnets, *Rep. Prog. Phys.* **29**, 285 (1966).
- [41] J. Nogués, J. Sort, V. Langlais, V. Skumryev, S. Suriñach, J. S. Muñoz, and M. D. Baró, Exchange bias in nanostructures, *Phys. Rep.* **422**, 65 (2005).
- [42] S. R. Huisman, R. V. Nair, A. Hartsuiker, L. A. Woldering, A. P. Mosk, and W. L. Vos, Observation of sub-Bragg diffraction of waves in crystals, *Phys. Rev. Lett.* **108**, 083901 (2012).
- [43] J. H. Han, P. X. Zhang, J. T. Hou, S. A. Siddiqui, and L. Q. Liu, Mutual control of coherent spin waves and magnetic, *Science* **366**, 1121 (2020).
- [44] O. Wojewoda, T. Hula, L. Flajšman, M. Vaňatka, J. Gloss, J. Holobrádek, M. Staňo, S. Stienen, L. Körber, K. Schultheiss, M. Schmid, H. Schultheiss, and M. Urbánek, Propagation of spin waves through a Néel domain wall, *Appl. Phys. Lett.* **117**, 022405 (2020).
- [45] P. Bödeker, A. Hucht, A. Schreyer, J. Borchers, F. Güthoff, and H. Zabel, Reorientation of spin density waves in Cr (001) films induced by Fe (001) cap layers, *Phys. Rev. Lett.* **81**, 914 (1998).

- [46] H. Zabel, Magnetism of chromium at surfaces, at interfaces and in thin films, *J. Phys. Condens. Matter* **11**, 9303 (1999).
- [47] I.D. Parker and A. Zettl, Spin-density-wave pinning in chromium, *Phys. Rev. B* **44**, 5313 (1991).
- [48] R. Hafner, D. Spisák, R. Lorenz, and J. Hafner, Does density-functional theory predict a spin-density-wave ground state for Cr?, *J. Phys. Condens. Matter* **13**, L239 (2001).
- [49] S. Wakimoto, R. J. Birgeneau, M. A. Kastner, and Y. S. Lee, Direct observation of a one-dimensional static spin modulation in insulating $\text{La}_{1.95}\text{Sr}_{0.05}\text{CuO}_4$, *Phys. Rev. B* **61**, 3699 (2000).
- [50] Y. Tsunoda, The commensurate-incommensurate SDW phase boundary of CrFe alloys, *J. Phys. Condens. Matter* **6**, 8513 (1994).
- [51] M. Mori, Y. Tsunoda, and N. Kunitomi, Strain wave in Cr rich CrFe alloys, *Solid State Commun.* **18**, 1103 (1976).